Towards Illumination-aware Visible Light Positioning Network Planning

Sander Bastiaens
INTEC - WAVES
Ghent University/imec
Ghent, Belgium
sander.bastiaens@ugent.be

Sotirios Goudos
ELEDIA@AUTH, Department of Physics
Aristotle University of Thessaloniki
Thessaloniki, Greece
sgoudo@physics.auth.gr

Wout Joseph
INTEC - WAVES
Ghent University/imec
Ghent, Belgium
wout.joseph@ugent.be

David Plets
INTEC - WAVES
Ghent University/imec
Ghent, Belgium
david.plets@ugent.be

2022 IEEE 12th International Conference on Indoor Positioning and Indoor Navigation (IPIN) | 978-1-7281-6218-8/22/$31.00 ©2022 IEEE | DOI: 10.1109/IPIN54987.2022.9918127

***Abstract*—A Visible Light Positioning (VLP) network planner holds tremendous economic potential in that it permits designing a roll-out within given cost, illuminance and accuracy bounds. In this manuscript, the Speed-constrained Multi-objective Particle Swarm Optimization (SMPSO) algorithm is applied to simultaneously optimise a roll-out's maintained illuminance and positioning error, by varying the placement of the VLP-enabled LED transmitters. With simulations that differ in positioning and/or environment parameters, the important illuminance-positioning trade-off is revealed. The corresponding Pareto fronts and LED arrangements are studied. Guidelines regarding where to place the LEDs and which LEDs to select for positioning are provided.**

***Index Terms*—Visible Light Positioning, VLP, Network Planning, LED locations, Optimization, Evolutionary Algorithm**

I. Introduction

Fitting with the 'circular economy' objective, the illumination market is transitioning towards the 'Light as a Service' (LaaS) business model. LaaS revolves around offering clients 'light' on a subscription basis, rather than selling them individual lamps. The LED lighting infrastructure remains the property and the responsibility of the illumination provider. With LaaS, illumination companies are accentuating energy efficiency and environmental-friendliness. Service differentiation, in order to gain a competitive advantage, paves the way for advanced light-based services such as 'human centric lighting' [1], Li-Fi [2] and *Visible Light Positioning (VLP)* [3].

The premise of a centimetre-order positioning accuracy in tandem with a low to medium price tag permits designating VLP as a promising next-generation indoor positioning technology. Its economic grounds do dictate that a lighting infrastructure, which is (projected to be) LED-dominated, is wielded to provide a concurrent positioning and illumination service. Within the field of VLP, many different system principles and components have been, and still are being developed. These differ among others in their: modulated light property (e.g. polarisation or intensity), transceivers, (de)modulation scheme, localisation paradigm (e.g. angle of arrival (AOA) or received signal strength (RSS)) and algorithm [3].

With economic viability as its primary incentive, this work focusses on indirect self-positioning RSS-based VLP, in which a single photodiode (PD)-based receiver localises itself with respect to an intensity modulated commercial off-the-shelf LED infrastructure. The PD directly detects broadcasted pilot symbols. This VLP system's simplex communication nature both minimises the required VLP-enabling lighting retrofit and the associated adoption hurdle, and permits a seamless receiver-side scalability. Prioritising cost-effectiveness, in conjunction with both a limited localisation complexity and the supporting of stroboscopic-prone applications, justifies the use of RSS with a PD-based receiver over AOA with a camera. Actually, VLP's positioning considerations do not proffer RSS with a sole PD per se. The absence of a synchronisation need, the minimal receiver device price tag, the constrained device feasibility, the low weight and the high obtainable update rate do render it well-suited for a wide range of applications.

The illumination-positioning synergy entails that transmitter anchor placement is an important parameter in the roll-out of a VLP system, perhaps even more so than for other indoor positioning systems. After all, the LED arrangement dictates both the illuminance distribution and the positioning coverage. Previous work [4] first studied the impact that the locations of the Lambertian LEDs have on the positioning performance solely. It employed the Grey Wolf Optimizer to plan the (sub)optimal LED layout for various roll-out configurations.

To also consider the vital symbiosis with the primary illuminance function, this manuscript extends [4] to incorporate a VLP roll-out's maintained illuminance E_m and illuminance uniformity U_0. The multi-objective optimisation problem, concurrently involving at least two of the positioning accuracy p_{10-90}, E_m and U_0 levels, is tackled with the Speed-constrained Multi-objective Particle Swarm Optimization (SMPSO) algorithm [5]. As optimisation objectives, the E_m/p_{10-90} relation is of particular interest, especially in view of illuminance uniformity U_0 and practical installation constraints. Nonetheless, the E_m/U_0 itself is considered too.

With SMPSO, a set of non-dominated solutions, i.e. the Pareto front, is brought forth. From these Pareto solutions, the 'optimal' transmitter layout can be chosen that adheres to an evaluation of the trade-off effectuated by a given set of objectives, i.e. the transmitter infrastructure is *planned*. The trade-off is a consequence of E_m, U_0, p_{10-90} tending to have

978-1-7281-6218-8/22/$31.00 ©2022 IEEE

contrasting effects on the LED locations. This manuscript reports planning results for 4 Lambertian LEDs with orders $m = 1$ or 5 that are placed either $h = 2$ m, 3 m, or 6 m above a PD receiver that is located in the standard square area of dimensions 5 m x 5 m. As positioning algorithms, trilateration and model-based fingerprinting (MBF) are studied [4].

Interestingly, comparing the Pareto solutions for the same environment, but for different lamp configurations that vary in their radiation pattern, permits identifying a suited VLP-enabled lighting design. Hence, guidelines can be derived regarding where to place what type of LED transmitters, in order to optimise a VLP roll-out amid different (environment) parameters. Finally, with this paper's methods and results, steps are taken in the design of a VLP network planner. The latter is instrumental to exploit VLP's full economic potential. A planner algorithm is discussed.

The main contributions of this paper can be condensed to:

- The investigation of the relation between the LED locations, the maintained illuminance E_m, the illuminance uniformity U_0 and the VLP positioning accuracy p_{10-90}.
- The provisioning of guidelines as to where to place the LED transmitters amid different environment parameters.
- A future perspective is given towards an industry-ready VLP network planner.

II. Related Work

A. Aspects to Illumination Planning

Solving the 'inverse lighting problem', in which optimal lighting locations and other parameters are searched for the resulting infrastructure to adhere to the applicable illumination regulations, has long been important, mainly for energy saving [6]. To enhance the light intensity, the uniformity, the shading effects and the costs of the illumination roll-out, genetic algorithms feature perhaps most prominently [7]. For example, Particle Swarm Optimization (PSO) solutions for lighting have been presented in [8], [9]. Evidently, none of these works considers non-lighting services, such as VLP.

B. Aspects to Light Positioning/Communication Planning

Within the context of Visible Light Communication (VLC), an algorithmic 2D optimisation of the LED locations in a practical environment is performed in [10]–[12]. In [10], Le et al. proposed an equilateral triangle distribution-based planning scheme. Singh et al. demonstrated that a more optimal signal-to-noise ratio (SNR) distribution can be obtained by not placing the 16 LEDs in a circular or square constellation [11]. Dastgheib et al. optimise the average throughput, subjected to a minimum illumination level and mobility rate, with an adaptive gradient projection algorithm [12]. A hexagonal arrangement is pointed to as being better suited for VLC.

Specifically for VLP, our pilot study [4] showed that the optimal LED arrangement is subject to the LED characteristics, the roll-out dimensions, and even the multipath contributions. For 2D trilateration in line-of-sight (LOS) conditions, with 4 LEDs in the 5 m by 5 m square room, the found arrangement is square. For other localisation algorithms, this is not necessarily the case. Importantly though, the trade-off between the illuminance and the positioning accuracy, and how it pertains to the LED locations, has not been extensively studied. This open issue is addressed by means of the materials and methods discussed next.

III. Materials and Methods

A. Multi-Objective LED Location Planning

As will be shown, a LED arrangement typically does not simultaneously optimise the maintained illuminance, the illuminance uniformity and the positioning accuracy. Therefore, the corresponding constrained multi-objective optimisation problem brings forth a set of non-dominated solutions, i.e. the Pareto Front. On the basis of Section II, the Speed-constrained Multi-objective Particle Swarm Optimization (SMPSO) [5] is chosen to generate the Pareto fronts with. SMPSO is an adaptive multidimensional extension of the Particle Swarm Optimization (PSO) algorithm. Analogous to the PSO formulation of [4], SMPSO's update rule reads:

$$u_{G+1,mk} = C\left[u_{G,mk} + c_{mk}\, r_{mk}\left(pb_{G+1,mk} - x_{G,mk}\right) + d_{mk}\, s_{mk}\left(gb_{G+1,mk} - x_{G,mk}\right)\right] \quad (1)$$

in which $x_{G,mk}$ and $u_{G,mk}$ denote the k^{th} particle's position and bounded velocity in the m^{th} dimension during the G^{th} iteration. $pb_{G,mk}$ and $gb_{G,mk}$ represent the particle's and the swarm's optimum objective function value, respectively. r_{mk}/s_{mk} and c_{mk}/d_{mk} are uniformly distributed random numbers in $[0, 1]$ and $[1.5, 2.5]$, respectively [13]. The velocity constriction factor C is there to favour convergence in case of swarm movement stoppage:

$$C = \frac{2}{\left|2 - \vartheta - \sqrt{\vartheta^2 - 4\vartheta}\right|} \quad (2)$$

with $\vartheta = c_{mk} + d_{mk}$ if $c_{mk} + d_{mk} > 4$. Otherwise, ϑ is set to 1. The default population size and iteration count are specified to be 40 and 150, respectively.

1) Objective Functions: Regarding the illuminance dimension, the objective functions to maximise are: the maintained illuminance E_m and the illuminance uniformity U_0. E_m and U_0 equal the spatial average, and the ratio between the spatial minimum and average illuminance, respectively. A lighting maintenance factor of 0.8 is computed with. With these metrics, it is important to note that in practical lighting design actually more in-depth parameters apply.

Regarding the positioning dimension, the objective is to minimise the p_{10-90} error over the evaluation grid (Section III-B). The p_{10-90} metric is defined as the area confined underneath 10% and 90% of the quantile function $\text{CDF}^{-1}(y)$, the inverse of the cumulative distribution function (CDF) of the positioning error y. y itself is defined as the Euclidean distance between the estimated and actual receiver location.

$$p_{10-90} = \int_{0.1}^{0.9} \text{CDF}^{-1}(y)\, dy \quad (3)$$

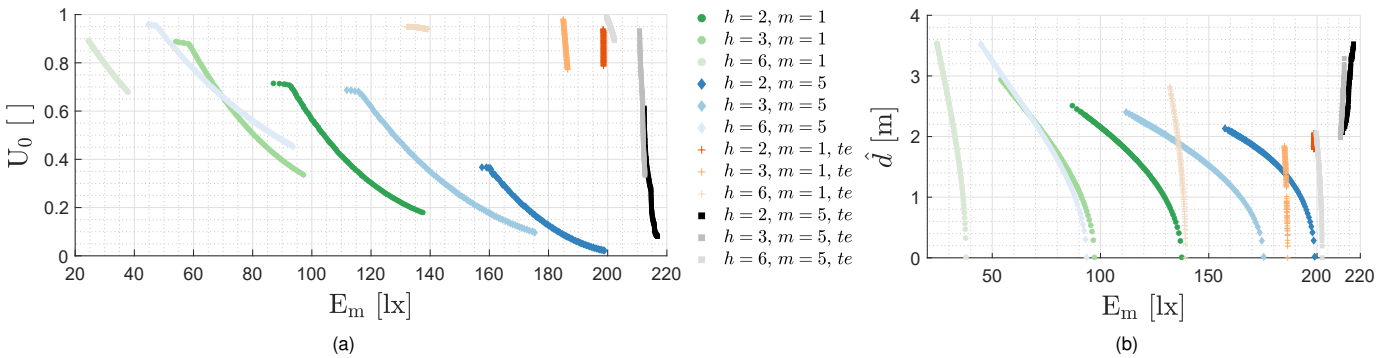

Fig. 1. SMPSO-based Pareto front representation of the (a) E_m- U_0 'illuminance' trade-off, exceptionally based on 300 iterations with 100 population members. Subfigure (b) shows the associated, optimised LED layouts' $\hat{d}$ as a function of E_m.

The rationale behind the p_{10-90} is that a single positioning percentile does not account for the shape of the CDF. For example, a solution in which every point on the positioning grid is characterised by the same positioning error of x cm exhibits an equal error percentile than a solution that only effectuates a non-zero error in that percentile of grid points. The integral limits are chosen for a more rapid solution convergence. They reject the grid points with an under/overvalued noise-induced error in a simulation. The p_{10-90} is averaged across 25 independent trials per objective function evaluation.

2) Fuzzy Decision Maker: To identify a best 'compromise' Pareto solution, the fuzzy membership function of (4) is turned to [14]. Each non-dominated solution $j = 1..M_{\text{par}}$ is assigned an overall satisfaction degree s_j:

$$s_j = \frac{\sum_{l=1}^{N_{obj}} sf_l^j}{\sum_{j=1}^{M_{\text{par}}} \sum_{l=1}^{N_{obj}} sf_l^j}, \; sf_l^j = \begin{cases} 1, \; z_l^j \geq z_l^{\max} \\ 1 - \frac{z_l^{\max} - z_l^j}{z_l^{\max} - z_l^{\min}}, \; \text{else} \\ 0, \; z_l^j \leq z_l^{\min} \end{cases} \quad (4)$$

z_l^j, $z_l^{\min}$ and $z_l^{\max}$ symbolise the j^{th} particle's, the minimum and the maximum value of the l^{th} of N_{obj} objective functions, respectively. The 'best' solution vector is taken as the one with the maximum s_j.

B. Propagation and Localisation Simulator

The considered simulation setup is similar to that of previous work [4]. The to be tracked object is equipped with an untilted PD-based receiver with an active area $A_R = 13 \text{ mm}^2$ to localise itself with respect to $N = 4$ white point source LEDs that are h metre higher up. Each LEDs' radiant flux $P_{t,i}, i = 1..N$ amounts to $P_t = 10$ W. The transceiver parameters match those of physical devices [4]. In the simulation experiments, a uniform evaluation grid with a 5 cm spacing is considered.

As is standard for VLP, the LOS model of Kahn et al. [15] is employed to simulate the propagation between the PD and a LED. Concretely, the PD's received radiant power contribution per LED $P_{R,i}$, i.e. the RSS value, is a function of $P_{t,i}$:

$$P_{R,i} = P_{t,i} \cdot R_E(\phi_i, \gamma_i) \cdot \frac{A_R}{d_i^2} \cdot \cos(\psi_i), \; |\psi_i| \leq \psi_C \quad (5)$$

where the symbols d_i, $R_E(\phi_i, \gamma_i)$, ϕ_i and γ_i, ψ_i and ψ_C represent the PD-LED$_i$ distance, LED$_i$'s radiation pattern, the elevation and azimuthal irradiance angles, and the PD's incidence angle and field of view. The $R_E(\phi_i, \gamma_i)$ of a Lambertian radiating point source simplifies to ${}^{(m_i+1)}/_{(2\pi)} \cos^{m_i}(\phi_i)$. $m_i = m$ denotes the Lambertian order.

Given the LED coordinates, the $\{P_{R,i}\}$ set and the propagation model, either least squares trilateration or model-based fingerprinting (MBF) on all $\{P_{R,i}\}$ is studied. For algorithmic details, previous work is referred to [4]. To simulate the positioning process, an additive and Gaussian input-referred current noise with a zero mean and a σ_I^2 variance is presumed. σ_I^2 is based on experiments [4]. To reduce the noise impact, per location estimate, 10 $P_{R,i}$ measurements are averaged.

The illuminance distribution is similarly computed to (5), though with a photometric interpretation. LED$_i$'s luminous flux $\Phi_i' = \Phi'$ is related to P_t via:

$$P_t = \frac{\Phi' \int_0^{2\pi} \left[\int_0^{\pi} R_E(\phi, \gamma) \sin(\phi) \, d\phi \right] d\gamma}{683.002 \int_{380}^{780} S(\lambda) \cdot V(\lambda) \, d\lambda} \cdot \int_{380}^{780} S(\lambda) d\lambda \quad (6)$$

in which $S(\lambda)$ and $V(\lambda)$ denote the LEDs' tabulated relative spectral power distribution and the human vision's luminosity function of Sharpe et al. [16] in nm, respectively. As, in line with [4], here, P_t represents a 50% duty cycle square wave magnitude, LED$_i$'s average luminous flux $\Phi_i = \Phi$ equals ${}^{\Phi'}/_2$: $\Phi = {}^{3302.6}/_2$ lm.

IV. Multi-Objective Planning Results

With SMPSO, Pareto-optimal LED arrangements are found that concurrently optimise illuminance and/or positioning objectives. The E_m, U_0 and p_{10-90} metrics are considered. The E_m/p_{10-90} trade-off is of particular interest, especially in relation to illuminance uniformity U_0 and practical installation constraints. However, the illuminance trade-off, i.e. E_m/U_0, is worth exploring too.

A. Exploring the Illuminance Requirements

Prior to delving into the $p_{10-90} - E_m$ relation, Fig. 1 (a) shows the interrelation between both illumination quantities, namely E_m and U_0, for 4 LEDs in the 5 m by 5 m by zone.

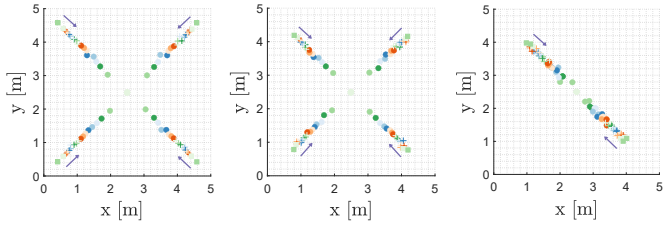

(a) $h = 3$ m, $m = 1$ (b) $h = 3$ m, $m = 5$ (c) $h = 6$ m, $m = 5$, te

Fig. 2. The SMPSO-optimised locations for $E_m - U_0$ in the case of (a) $h = 3$ m and $m = 1$ and (b) $h = 3$ m and $m = 5$. Subfigure (c) depicts the optimised tessellation locations for $h = 6$ m and $m = 5$.

Each Pareto solution of a particular Pareto front represents the optimised LED arrangement for that E_m and U_0 combination. All Pareto curves highlight that for Lambertian LEDs the illuminance uniformity U_0 decreases when the maintained illuminance E_m increases.

The rationale is apparent when examining the corresponding LED locations by means of Fig. 2 (a)-(b). These figures display the locations of 25 SMPSO solutions for (a) $h = 3$ m/$m = 1$ and (b) $h = 3$ m/$m = 5$. They are selected to cover the U_0 range with equal spacing. In Fig. 2, starting at the minimal U_0, the colour and marker sequence are green/blue/red, with for each colour 3 shades that are ranked from lightest to darkest, and bullet/plus sign/square, respectively. Hence, the arrows indicate a decreasing U_0, and consequently an increasing E_m.

The main takeaways from Fig. 1 and Fig. 2 (a)-(b) are that regardless of h/m: (i) the Pareto solutions form near-square arrangements and (ii) a decreasing U_0/enlarging E_m is accompanied by a monotonic shrinking of the square's dimensions. This shrinking effect is spotlighted in Fig. 1 (b) by plotting each constellation's $\hat{d}$, which is the mean of the 4 LEDs' Euclidean distance to the room's centre. The highest E_m is obtained when the LEDs flock together, i.e. forming a white spot. Elevated degrees of uniformity then move the locations outwards, to enlarge the illuminance at the zone's outskirts. The maximal $\hat{d}$ value, associated with the largest obtainable U_0, depends on m and the dimensions (specifically on h here). The latter links to the maximal ϕ_i/γ_i involved.

Interestingly, the monotonicity of $E_m - \hat{d}$ permits wielding a curve fit to analytically compute the optimal $\hat{d}$, given a roll-out's dimensions, transmitter radiation pattern and E_m ($\bar{E}_m$) and U_0 ($\bar{U}_0$) targets. Moreover, the specificity of the $E_m - \hat{d}$ curves allows selecting the desired LEDs for new roll-outs. Thus, lighting design can be performed.

Finally, it needs to be remarked that these conclusions do not necessarily apply to arbitrary LEDs and roll-outs. For asymmetrically-radiating LEDs, the $E_m - U_0$ curve's range and shape may differ from Fig. 1's. Though, to reach maximal E_m, $\hat{d}$ typically converges to 0. For various illumination-type LEDs, the arrangement tends to become rectangular-like due to radiation pattern symmetry. A growing U_0 then may no longer induce a dimension-invariant, outward shift of the LEDs. The preservation of the constellation's shape is not guaranteed.

1) A 4-LED Base Cell in a Large-scale Infrastructure: With the exception of small residential or office-type of environments, seldom, a 4-LED configuration suffices to provide adequate illuminance coverage. In fact, large-scale illumination deployments tend to be formed as a tessellation of, in this case, 4-LED square basic cells. This part investigates the extent of the impact that the 8-nearest neighbour basic cells, all with 4 LEDs and a 5 m by 5 m area, have on the considered basic cell's LED location distribution.

Referred to with te, these tessellation $E_m - U_0$ curves are also depicted in Fig. 1 (a). The $E_m - U_0$ relations still descend with an increasing E_m. Evidently, higher E_m/U_0 values and a smaller E_m variation range are obtained due to the risen LED density. Moreover, the maximum m to ensure adequate uniformity increases, which will benefit the positioning. Comparing Fig. 2 (a)/(b) and Fig. 2 (c) allows concluding that for the m/h configurations under test, with the periodic extension, the previously planned arrangements are typically not Pareto optimal. Fig. 2 (c) demonstrates that the LED arrangement can diverge from the square. In this case, a composition (near) square constellation over the cell bounds is formed. Interestingly, SMPSO may moreover return multiple LED location shapes for a given roll-out, which are optimal in a certain E_m/U_0 range. When maximising U_0 for example, solutions with hexagonal LED coverage areas are frequent.

Naturally, the $\hat{d}$ behaviour depends on m and the environment dimensions, as attested by Fig. 1 (b). Importantly though, with tessellation, $\hat{d}$ does not necessarily drop to zero. Roll-outs exist for which maximising E_m does not entail grouping the LEDs. As a side note, some m/h cases, i.a. $h = 3$ m and $m = 5$ feature a $\hat{d} > 1.5$ m irrespective of E_m/U_0 as a consequence of their LED locations not being centred in the 5 m by 5 m zone.

B. VLP Network Planning with Unconstrained LED Locations

The Pareto fronts of Fig. 3 (a) visualise VLP's $p_{10-90} - E_m$ trade-off, for various roll-out configurations. Fig. 3 (b) and Fig. 4 show the corresponding $\hat{d}$ evolution and the associated influence on the LED locations, represented by 25 p_{10-90}-uniformly selected final population members, respectively.

Fig. 3 (a) reveals that a roll-out solely optimised in terms of the p_{10-90} performance inadvertently compromises on the obtainable E_m. A better tuned E_m in turn incurs a p_{10-90} penalty. Fig. 4 attests that, as was the case in Section IV-A, an increasing E_m effectuates an inward shrinking of the LED arrangement, whilst approximately maintaining the shape. The LED constellations associated with the optimal p_{10-90} score, match those of previous work [4]. For trilateration, they are (near) squares with their sides parallel to the zone's outlines [Fig. 4 (a)-(e)]. For MBF, a 45° rotated version is found [Fig. 4 (f)]. Moreover, the maximal $\hat{d}$, corresponding to this minimal p_{10-90}, again logically depends on the VLP roll-out [Fig. 3 (b)]. It shrinks for a rising m and decreasing h. When contrasting Fig. 1 (b) and Fig. 3 (b), a larger maximal $\hat{d}$ is perceived when optimising for U_0 instead of for p_{10-90}.

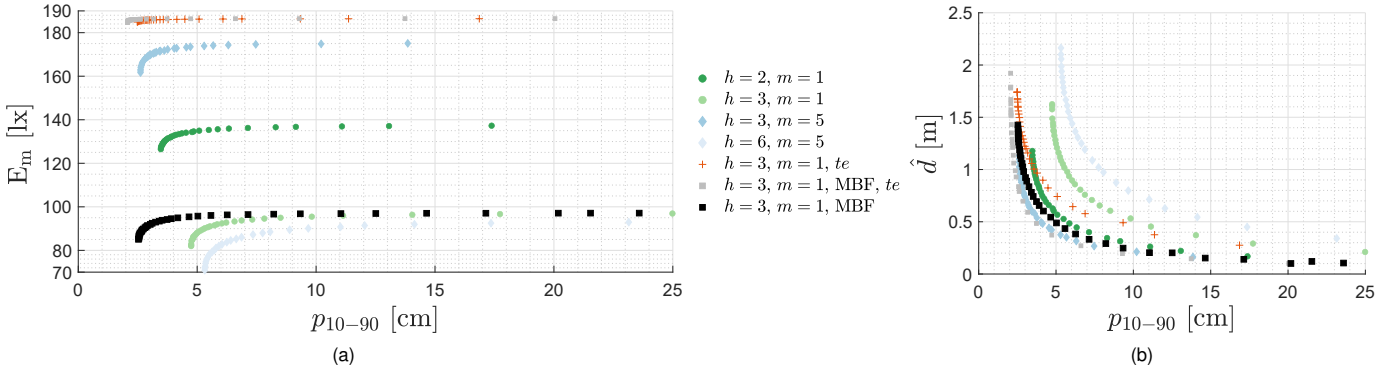

Fig. 3. SMPSO Pareto front representation of the (a) $p_{10-90} - E_m$ 'positioning' trade-off and its associated (b) Pareto optimal $\hat{d}$ as a function of p_{10-90}.

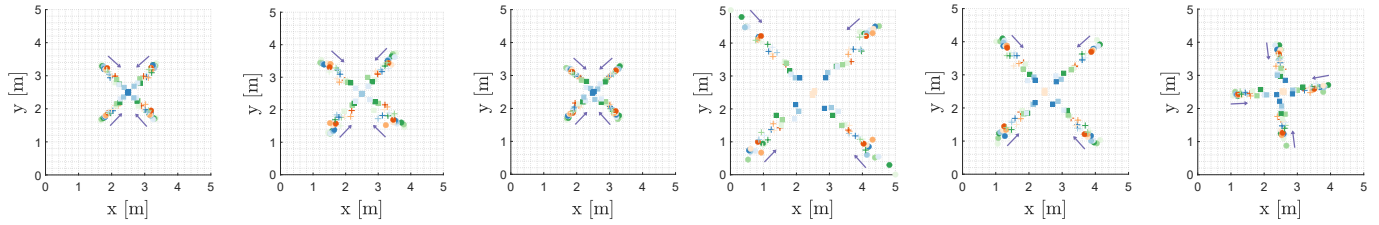

(a) $h = 2$ m, $m = 1$ (b) $h = 3$ m, $m = 1$ (c) $h = 3$ m, $m = 5$ (d) $h = 6$ m, $m = 1$ (e) $h = 6$ m, $m = 5$ (f) $h = 3$ m, $m = 1$, MBF

Fig. 4. The influence of the $p_{10-90} - E_m$ on the LED locations for trilateration with (a) $h = 2$ m and $m = 1$, (b) $h = 3$ m and $m = 1$, (c) $h = 3$ m and $m = 5$, (d) $h = 6$ m and $m = 1$, (e) $h = 6$ m and $m = 5$ and for MBF with (f) $h = 3$ m and $m = 1$. The purple arrows indicate the LED locations' evolution in response to a growing E_m.

Optimising an illumination-compliant VLP roll-out thus entails an illuminance coverage versus positioning accuracy trade-off. Here, the $p_{10-90} - E_m$ can in the (co)domain by approximation be modelled as $a - {}^{b}/_{(c+x)^d}$, with a, b, c and d numerical parameters. Thus, again, the curve fitting of Fig. 3 allows a numerical evaluation of the $p_{10-90} - E_m$ trade-offs.

On the basis of Fig. 3 (a), the following guidelines can be asserted. (i) Within bounds, both a roll-out's p_{10-90} and E_m benefit from employing Lambertian LEDs with a higher order m and the associated increased $P_{R,i}$ gradient. However, an upper bound m value can be identified, beyond which the 4 LEDs are unable to provide a sufficient SNR/p_{10-90} coverage. This phenomenon occurs for $h = 2$ m and $m = 5$. The maximal m value m_{max} is environment-dependent. The latter's dimensions dictate the maximal opening angle/aperture, for which the radiance and luminous flux needs to be maximised. For the same positioning area, m_{max} increases when h enlarges. (ii) In line with [4], MBF is able to deliver a lower p_{10-90} for an equal E_m with respect to trilateration, when it is considered both for planning and positioning. Moreover, its minimum E_m exceeds that of trilateration, rendering it a slightly better positioning algorithm.

Intriguingly, Section III-A2 permits identifying a single compromise solution per $p_{10-90} - E_m$ front. $E_m = 96.9$ lx/$p_{10-90} = 25.0$ cm and $E_m = 96.3$ lx/$p_{10-90} = 6.3$ cm for $h = 3$ m/$m = 1$ with trilateration and MBF, respectively. The significant concessions on the p_{10-90} are a result of the large p_{10-90} range, with values up to and exceeding 1 m. As in practice the importance of the positioning tends to outweigh that of the illuminance, a p_{10-90} curbing is proposed. Rather than a reweighing of Section III-A2's (4), the maximal p_{10-90} is constrained to 10 cm. Now, the best compromise solution amounts to $E_m = 92.0$ lx/$p_{10-90} = 5.8$ cm and $E_m = 94.5$ lx/$p_{10-90} = 3.9$ cm for trilateration and MBF.

In line with Section IV-A, these $p_{10-90} - E_m$ conclusions are not necessarily valid for arbitrary LEDs and roll-out dimensions. In fact, for MBF (trilateration performs vastly inferior) in the 5 m by 5 m area, asymmetrically-radiating LEDs may feature in a 1D stretched rhombus-like version of Fig. 4 (f), in a rectangle, ..., with the exact nature depending on their radiation patterns. What is also worth mentioning is that $p_{10-90} - E_m$-profits can be had, over $m = 1$ (and $m = 5$), by employing illumination-type LEDs that are designed for higher U_0 and for more-glare-stringent applications, provided that their placement is optimised. The $p_{10-90} - E_m$ itself may vary in curvature and shape from the Lambertians'.

1) A 4-LED Cell in a VLP Network: Fig. 3 also renders the $p_{10-90} - E_m$ curves (denoted by te) in the VLP network case, i.e. when the 4-LED cell is encompassed by its 8 adjoining basic cells. Evidently, the neighbours' influence ensures a substantially improved p_{10-90} and E_m (upper curves). It is a consequence of the additional $P_{R,i}$ coverage at the zone's edges and corners. Interestingly, the performance gap between trilateration and MBF significantly narrows as well. Fig. 5 (a)/(b) shows the tessellation's influence on the LED constellations of $h = 3$ m/$m = 1$ for trilateration/MBF. In

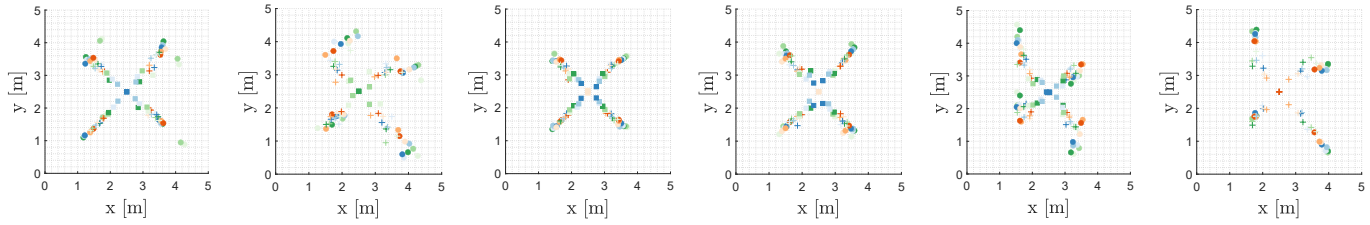

Fig. 5. The influence of (a)/(b) the periodic LED arrangement extension, (c)/(e) the rail constraint and of (d)/(f) the conjoint presence of railing and tessellation, on the LED locations pertaining to the $p_{10-90} - E_m$ trade-off for $h = 3$ m and $m = 1$, with (a)/(c)/(d) trilateration and (b)/(e)/(f) MBF, respectively.

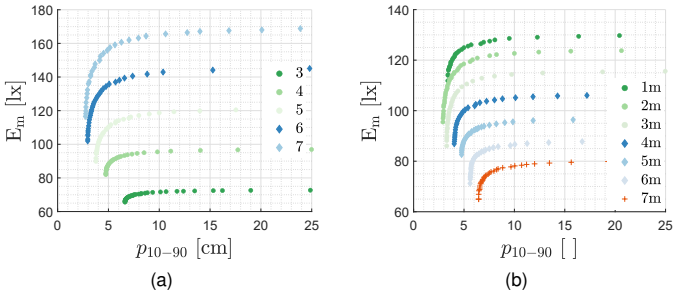

Fig. 6. The $p_{10-90} - E_m$'s sensitivity to (a) the LED count and (b) the one-sided scaling of the environment with a fixed dimension of 5 m.

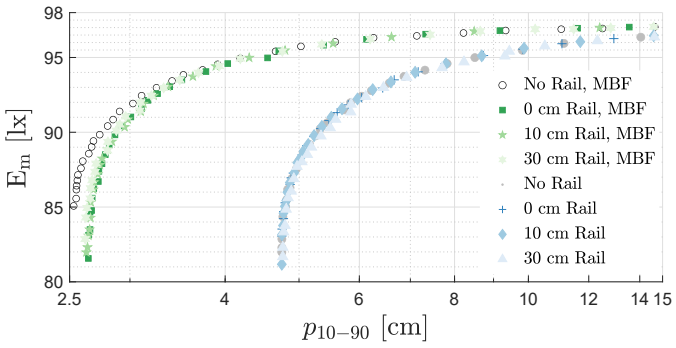

Fig. 7. The influence of the rail width on the $p_{10-90} - E_m$ Pareto fronts for $h = 3$ m and $m = 1$.

particular, the MBF locations are impacted. They skew and rotate with tessellation. Composition LED arrangements form.

2) Miscellaneous: As stated, the trilateration $p_{10-90} - E_m$ is impacted by not-h roll-out factors as well, such as the LED density, the 2D environment size and the optimisation metric. Fig. 6 (a) displays that adding LEDs to the 5 m x 5 m area, evidently ensures a $p_{10-90} - E_m$ improvement. Nonetheless, noise effectuates a progressively narrowing p_{10-90} benefit. The associated arrangements match those of [4]. Fig. 6 (b) shows the expected, diagonally downwards $p_{10-90} - E_m$ shift, when one room dimension stretches. The 'optimal' LED arrangements are generally not square, for a not-square area. They are skewed to be parallelogram-like, stretching in the longest room dimension. Importantly, for rooms with a large aspect ratio, the reduced, obtainable dilution of precision (DOP) will constrain the achievable p_{10-90}. There, to optimise the DOP and the p_{10-90}, the LEDs are pushed to the zone's edges. Finally, as was the case in [4], the chosen optimisation metrics affect the resulting trade-off and associated LED locations sets. For instance, maximising the minimal illuminance sees the LEDs moving outwards with a decreasing p_{10-90}.

C. Practical LED Placement Constraints and VLP

The prototypical LED transmitter's power consumption both prohibits battery-powered operation and requires interfacing with the mains voltage. With due consideration of installation/cost-efficiency, therefore, lights tend to be installed in single file, i.e. on rails, tracks or cable trays. Hence, in practical deployments, the transmitter placement is location-constrained. Fig. 7 depicts the $p_{10-90} - E_m$ for $h = 3$ m and $m = 1$ when the placement is restricted to either of 2 rails, each with a width of either 0 cm, 10 cm or 30 cm. Fig. 5 (c)/(e) shows the associated placements for the former.

With trilateration preferring a square constellation [4], the rail constraints do not negatively affect the $p_{10-90} - E_m$. On the contrary, enforcing the pairwise x-coordinate restrictions confines the search space. The effect on the MBF planned locations and positioning is more profound, as indicated by Fig. 5 (e) and Fig. 7. The stricter the location constraint, i.e. the smaller the rail width, the less optimal the $p_{10-90} - E_m$ is. A line rail induces a p_{10-90} increase of approximately 0.1 cm for equal E_m values, with respect to the unconstrained case. It corresponds to 4% when the position dimension is optimised. For higher E_m, this p_{10-90} cost loses relevance. As a side note, technically, the unconstrained LED arrangement of Fig. 4 (f) can be installed by 'diagonally' placing the lighting rails. However, this is not prevalent. Finally, in the tessellation configuration, the penalty associated with lighting rails is limited. The planned locations are visualised in Fig. 5 (d) and (f) for trilateration and MBF, respectively.

D. Illuminance Uniformity Constraints for VLP

Section IV-B treated the $p_{10-90} - E_m$ trade-off, without considering the (legally) imposed illuminance bounds. In practice, lighting standards or directives, such as the European EN 12464-1, dictate a minimal $\bar{E}_m$ and $\bar{U}_0$ for a given task appertaining to a certain application. Naturally, these metrics apply for illumination-compliant VLP networks as well. $\bar{E}_m$ can be accounted for via the $p_{10-90} - E_m$ curve. The additional influence of a $\bar{U}_0$ constraint is charted by means of Fig. 8.

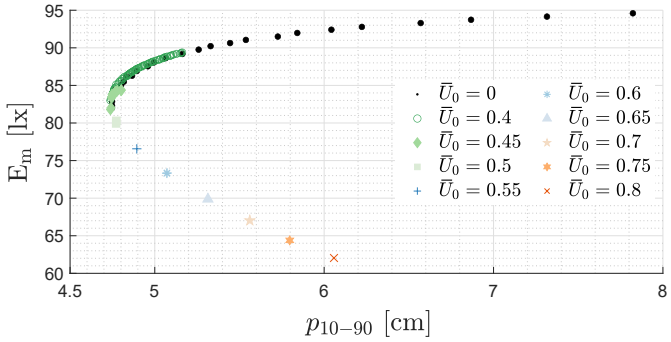

Fig. 8. The attainable $p_{10-90} - E_m$ Pareto solutions with trilateration and for $h = 3$ m/$m = 1$, under different illuminance uniformity constraints $\bar{U}_0$.

Lenient $\bar{U}_0$ constraints render the part of the Pareto solutions range with a better p_{10-90} still admissible for deployment. The lower $\bar{U}_0$, the larger the admissible p_{10-90}/E_m range. For $h = 3$ m and $m = 1$, $\bar{U}_0 = 0.4$, applicable in e.g. passage, storage rack or robotics areas, is still reachable.

With more stringent $\bar{U}_0$ lower bounds, found in areas with frequent visual tasks, a different story arises. The Pareto front then comprises one solution. $\bar{U}_0$ then unambiguously dictates the LEDs' location. It typically requires the LEDs to be further apart than what is ideal for positioning. Obviously, the lenient/stringent distinction $\bar{U}_0$ value depends on the roll-out.

V. Discussion

A. Guidelines

Based on this work, the following can be recommended for planning an illuminance-compatible VLP roll-out:

- The Pareto transmitter placement solutions of the monotone E_m–U_0 are square in nature in a square room, which fits particularly well with trilateration. In a tessellation configuration, the LED locations may form a composition constellation with the neighbouring cells' locations.
- Jointly considering E_m and p_{10-90} reveals an important trade-off. Optimising the p_{10-90} returns the LED constellations of [4] that are (near-)squares for trilateration, whilst enlarging the E_m makes the LEDs' arrangement shrink towards to the room's centre.
- Adequately modelling the Pareto front and the associated $\hat{d}$ curves permits a lighting design, by selecting the appropriate trade-off solution from different LED configurations. For Lambertian LEDs, below a maximum, the $p_{10-90} - E_m$ profits from higher m values.
- When the 4-LED coverage area features in a tessellation configuration, the shape of the Pareto LED locations tends to differ.
- The rail constraint only affects MBF's solutions. The trilateration and tessellation te solutions are not hindered.
- Above a roll-out-specific $\bar{U}_0$ threshold, $\bar{U}_0$ unilaterally dictates the LED locations. The Pareto front comprises but a single point. Below that $\bar{U}_0$ limit, a range of the unconstrained solutions is validated for use.
- The 'white spots' associated with Lambertian LEDs prohibits their utilisation for high $\bar{U}_0$ applications.

B. Design of a Future Network Planner

As stated in the introduction, predicting the installation cost and the tracking accuracy, and performing automatic constrained design, of a prospective VLP roll-out holds tremendous economic value. This work only provides a stepping stone towards this network planner. Other stones comprise:

1) In-depth Illumination Planning: As mentioned in Section III-A1, illumination standards, such as EN 12464-1, actually dictate more in-depth parameters than a single $\bar{E}_m$ and $\bar{U}_0$ value per room. Typically, varying activity areas will be characterised by different requirements, which depend on the visual task at hand. By specifying the requirements as constraints in the planning, these can be accounted for.

2) Nature of the Infrastructure: VLP's cost dimension depends on whether a prior illumination infrastructure is present. Therefore, the tool should support investigating/planning a VLP-dedicated, in the form of a new or appended installation, a changeover or a hybrid infrastructure. To enable the latter, the tool permits the locations of the present lamps to feature as constraints. Herewith, it is noted that as a consequence of the VLP-enabling, the nature of the activity area and the corresponding illuminance constraints may change. For example, through the ensuing automation, a factory hall no longer needs human involvement. This impacts the number of LEDs that need to be VLP-enabled.

3) Extension to 3D Localisation with Arbitrary LEDs: Supporting 3D positioning with arbitrary light sources is straightforward. To not having to compute a fine evaluation grid for each LED constellation, either the DOP or a sparse model is best computed. Due to the position ambiguity found with Lambertian-like LEDs [17], the optimal 3D constellation will differ from that of 2D trilateration positioning. To break this ambiguity, the transmitters' height and/or tilt dimension should be considered too.

4) Anchor Density Trade-off: With the planning tool, the influence of the anchor density on VLP's illuminance-cost-accuracy trade-off can be charted. The consequent results will both dictate how many LEDs need to be provisioned for a certain environment, and characterise the to be expected cost of a VLP roll-out per square metre.

5) Planning an Industry-size Roll-out: In this work, the infrastructure was of limited scale. For large roll-outs, a 3-step network planner is envisioned. The three steps are:

a) Initial environment covering: The application's budget-accuracy requirement and the illuminance constraints point to a certain LED density. The idea is hereto to rely on both the lumen method and the relationship between a Pareto solution and its corresponding LED locations (Section IV-B). Once obtained, the LED density is then translated into a (sub)optimal base propagation cell, e.g. 4 LEDs per 5 m by 5 m area. A heuristic then fills the LED plane, starting from a room corner. At each epoch, a single basic cell is selected from a precomputed database. This database also holds all its

variants that are characterised by being flanked by a different configuration of cell neighbours (e.g. 1 left, or a top and a bottom neighbour). Each has a priori optimised transmitter locations. Gradually, a global transmitter infrastructure composed of basic configurations, and its associated propagation model approximation is obtained.

Due to symmetry, the number of database entries can greatly be reduced. Should a certain cell type be missing, the propagation code is run and the new cell is added to the database. To limit the online computations, basic cells that comprise various wall configurations, with 1/2/3 or 4 walls of a certain material, can be provisioned too.

b) LOS planner: The initial covering is superseded by a full-fledged planning algorithm. Whereas obstacles were previously ignored, in this second step, they are approximated by their bounding box and only their light obstruction function is accounted for. To limit the computational complexity, obstacle details are hence disregarded. After a predefined number of iterations, in which the evaluation grid density is restricted by means of sparsity techniques, such as surrogate models [18], the SMPSO algorithm then outputs a second intermediary LED constellation. The DOP suffices as cost function. All solutions not adhering to the pre-set illumination requirements are rejected.

c) NLOS optimiser: The third and last subfunction accounts for the multipath components introduced by obstacles. A limited amount of SMPSO iterations are ran to slightly, i.e. within (lighting rail) bounds, adapt the LED coordinates of those in the $1.5\ \mathrm{m}$ vicinity of these obstacles. The computation of the NLOS contributions is also confined to that zone. The $1.5\ \mathrm{m}$ bound is based on prior experiments. Once more, spatially-confined sparse models are wielded. To ascertain that the planner's output closely matches with the practical deployment, relevant noise and interference models are an absolute necessity.

VI. Conclusion & Future Work

This manuscript addressed the research problem of where to (sub)optimally place the LED transmitters in PD RSS-based VLP. The multi-objective problem of concurrently tailoring a VLP roll-out's illumination and positioning levels was tackled with the Speed-constrained Multi-objective PSO (SMPSO) evolutionary optimisation algorithm. The, with SMPSO obtained, Pareto fronts highlighted the manifestation of a maintained illuminance $E_m - p_{10-90}$ trade-off. These fronts were shown to permit lighting design with (Lambertian) LEDs. The influence of practical constraints, in terms of installation or illuminance uniformity, on the Pareto solutions was studied. Finally, an outline was provided towards the development of an industry-ready VLP network planner.

The future work mainly entails ameliorating and extending, e.g. by including AOA VLP, the above network planning tool. With it, the quality of positioning service metrics of VLP's different system principles can be analysed. Definitive answers can then be found for: "Is it more interesting to add a VLP-dedicated point source to an illumination infrastructure, or rather to retrofit it either in part or in its entirety?", "How many LEDs need to be VLP-enabled?", etc.

References

[1] K. Zielinska-Dabkowska, "Make lighting healthier," in *Nature*, vol. 553, pp. 274–276, 2018, doi: 10.1038/d41586-018-00568-7.

[2] H. Haas, L. Yin, Y. Wang and C. Chen, "What is LiFi?," in *Journal of Lightwave Technology*, vol. 34, no. 6, pp. 1533–1544, 2016, doi: 10.1109/JLT.2015.2510021.

[3] Y. Zhuang et al., "A Survey of Positioning Systems Using Visible LED Lights," in *IEEE Communications Surveys & Tutorials*, vol. 20, no. 3, pp. 1963–1988, 2018, doi: 10.1109/COMST.2018.2806558.

[4] S. Bastiaens, S. K. Goudos, W. Joseph and D. Plets, "Metaheuristic Optimization of LED Locations for Visible Light Positioning Network Planning," in *IEEE Transactions on Broadcasting*, vol. 67, no. 4, pp. 894–908, 2021, doi: 10.1109/TBC.2021.3099734.

[5] A. J. Nebro, J. J. Durillo, J. Garcia-Nieto, C. A. C. Coello, F. Luna and E. Alba, "SMPSO: A new PSO-based metaheuristic for multi-objective optimization," *IEEE Symposium on Computational Intelligence in Multi-Criteria Decision-Making (MCDM)*, Nashville, TN, USA, Mar. 30 - Apr. 2, 2009, pp. 66–73, doi: 10.1109/MCDM.2009.4938830.

[6] Y.-J. Wen and A. Agogino,"Control of wireless-networked lighting in open-plan offices," in *Lighting Research & Technology*, vol. 43, no. 2, pp. 235–248, 2011, doi:10.1177/1477153510382954

[7] F. Cassol, P. S. Schneider, F. H. França and A. J. S. Neto, "Multi-objective optimization as a new approach to illumination design of interior spaces," in *Building and Environment*, vol. 46, pp. 331–338, 2011, doi: 10.1016/j.buildenv.2010.07.028.

[8] P. Mandal, D. Dey and B. Roy, "Optimization of luminaire layout to achieve a visually comfortable and energy efficient indoor general lighting scheme by Particle Swarm Optimization," in *LEUKOS: The Journal of the Illuminating Engineering Society*, vol. 17, no. 1, pp. 91–106, 2021, doi: 10.1080/15502724.2018.1533853.

[9] J.-Q. Qu, Q.-L. Xu and K.-X. Sun, "Optimization of Indoor Luminaire Layout for General Lighting Scheme Using Improved Particle Swarm Optimization," in *Energies*, vol. 15, no. 4, p. 1482, pp. 1–18, 2022, doi: 10.3390/en15041482.

[10] Z. Le, X. Zeng and M. Fu, "Optimized Base Station Location Planning for Indoor Positioning in Visible Light Communication System," in *Journal of Optical Communications*, vol. 39, no. 4, pp. 437–447, 2017, doi: 10.1515/joc-2017-0004.

[11] A. Singh, A. Srivastava, V. A. Bohara and G. S. V.R.K. Rao, "Performance of Indoor Visible Light Communication System Under Random Placement of LEDs," *21st International Conference on Transparent Optical Networks (ICTON)*, Angers, France, July 9-13, 2019, pp. 1–5, doi: 10.1109/ICTON.2019.8840427.

[12] M. A. Dastgheib, H. Beyranvand and J. A. Salehi, "Optimal Placement of Access Points in Cellular Visible Light Communication Networks: An Adaptive Gradient Projection Method," in *IEEE Transactions on Wireless Communications*, vol. 19, no. 10, pp. 6813–6825, 2020, doi: 10.1109/TWC.2020.3006204.

[13] T. T. Truong, J. Lee and T. Nguyen-Thoi, "Multi-objective optimization of multi-directional functionally graded beams using an effective deep feedforward neural network-SMPSO algorithm," in *Structural and Multidisciplinary Optimization*, vol. 63, pp. 2889–2918, 2021, doi: 10.1007/s00158-021-02852-z.

[14] C. Carlsson and R. Fullér, "Fuzzy multiple criteria decision making: Recent developments," in *Fuzzy Sets and Systems*, vol. 78, no. 2, pp. 139–153, 1996, doi: 10.1016/0165-0114(95)00165-4.

[15] J. M. Kahn and J. R. Barry, "Wireless infrared communications," in *Proceedings of the IEEE*, vol. 85, pp. 265–298, 1997, doi: 10.1109/5.554222.

[16] L. T. Sharpe, A. Stockman, W. Jagla and H. Jägle, "A luminous efficiency function, $V^\star(\lambda)$, for daylight adaptation," in *Journal of Vision*, vol. 5, pp. 948–968, 2005, doi: 10.1167/5.11.3.

[17] D. Plets, Y. Almadani, S. Bastiaens, M. Ijaz, L. Martens and W. Joseph, "Efficient 3D Trilateration Algorithm for Visible Light Positioning," in *Journal of Optics*, vol. 21, no. 5, pp. 1–4, 2019, doi: 10.1088/2040-8986/ab1389.

[18] D. Gorissen, K. Crombecq, I. Couckuyt, T. Dhaene and P. Demeester, "A Surrogate Modeling and Adaptive Sampling Toolbox for Computer Based Design," in *Journal of Machine Learning Research*, vol. 11, pp. 2051–2055, 2010.

2022 International Conference on Indoor Positioning and Indoor Navigation

IEEE Catalog Number: CFP2209J-ART
ISBN: 978-1-7281-6218-8

2022 IEEE 12th International Conference on Indoor Positioning and Indoor Navigation (IPIN) | 978-1-7281-6218-8/22/$31.00 ©2022 IEEE | DOI: 10.1109/IPIN54987.2022.9918140

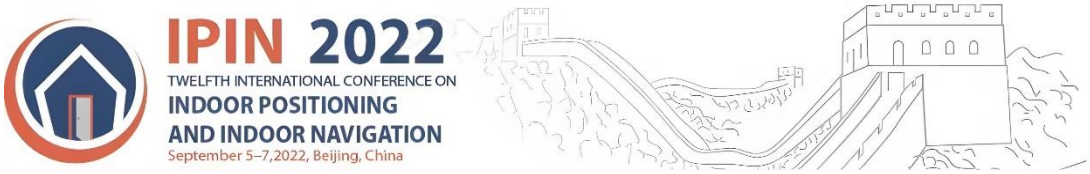

12th International Conference on Indoor Positioning and Indoor Navigation

IPIN 2022

September 5-7, 2022, Beijing, China

http://www.ipin-conference.org/2022/

Organized by

Aerospace Information Research Institute (AIR),
Chinese Academy of Sciences (CAS)

2022 IEEE 12th International Conference on Indoor Positioning and Indoor Navigation (IPIN) | 978-1-7281-6218-8/22/$31.00 ©2022 IEEE | DOI: 10.1109/IPIN54987.2022.9917512